Lattice-dynamical and photoelastic properties of GaSe under high pressures studied by Raman scattering and electronic susceptibility

Noritaka Kuroda, Osamu Ueno,* and Yuichiro Nishina
The Research Institute for Iron, Steel and Other Metals, Tohoku University, 2-1-1 Katahira, Sendai 980, Japan
(Received 17 October 1986)

Raman scattering and infrared studies are reported for the layer compound GaSe under hydrostatic pressures up to 4 GPa. The rigid-layer mode shifts towards higher frequencies with an initial pressure coefficient of 0.234 GPa^{-1}. The overall behavior is explained in terms of the volume anharmonicity characteristic of the van der Waals bonding. The internal bond-bending mode softens and the Born effective charge decreases linearly. By adopting the single-layer compressibility $\kappa_l \simeq 0.015$ GPa^{-1} we obtain a Grüneisen parameter of -1.9 for the bond-bending mode and -0.55 ± 0.05 for the effective charge, comparable to those of a tetrahedral semiconductor. Coexistence of such molecular and covalent characters leads to a nonlinear shift of the energy, E_g, of the Penn-Phillips oscillator. This behavior is shown to be described well by $\Delta E_g = D_a(\Delta a/a_0) + D_c(\Delta c/c_0)$ with the deformation potentials $D_a = -7.6 \pm 1.0$ eV for the **a** axis and $D_c = 1.06 \pm 0.16$ eV for the **c** axis. These deformation potentials reflect the dimensionality of bonding network as well as the nature of the electronic structure.

I. INTRODUCTION

The dependence of the phonon spectrum on hydrostatic pressure has been studied for many semiconductors since Mitra *et al.* reported the pressure dependence of the first-order Raman spectra in ZnO, ZnS, ZnSe, ZnTe, CdS, GaP, and SiC.[1,2] Their works demonstrate that (1) the TO and LO modes shift towards higher frequency with pressure, (2) the magnitude of the LO-TO splitting decreases with pressure, the rate being higher with higher ionicity, and (3) in wurtzite-type materials such as CdS and ZnO, the E_2 mode which corresponds to the TA mode at the L point of the Brillouin zone of the zinc-blende-type materials shifts towards lower frequency. Hochheimer *et al.* have obtained similar results for the behavior of LO and TO modes in CuCl, CuBr, and CuI.[3] Cardona and his co-workers have paid attention to the Born effective charge in GaAs, InP, GaSb, InAs, and InSb.[4–6] The Born effective charge decreases with pressure in a fairly general way, indicating that the polarity and thus the ionicity decreases upon contraction of the tetrahedral bonding.

Subsequently, the second-order Raman spectrum has been measured in Si, Ge, 3C-SiC, GaP, ZnS, ZnSe, and ZnTe.[7–10] In these cubic materials, the TA mode at the zone boundary softens remarkably under pressure. This phenomenon is consistent with the observation by Mitra *et al.* for the TA_L-like mode in CdS and ZnO. The softening of short-wavelength TA phonons is reminiscent of the decrease in the bending force of a tetrahedral bond. Weinstein has conceived it as the driving mechanism of the transformation into a metallic phase which takes place in a tetrahedral semiconductor at a high pressure.[9]

The bond charge is principally responsible for the screening of the potential between constituent atoms. The role of the bond charge on the behavior of phonons under pressure has been theoretically studied by means of various approaches based on pseudopotentials.[11–13] It has been clarified throughout these works that delocalization, deformation, and displacement of the bond charge cause a change in the strength of the screening so as to increase the central force and to decrease the noncentral force.[14] In particular, the noncentral force which determines the frequency of the zone-boundary TA mode has been argued to be very short range. These theoretical results agree well with experimental findings mentioned above as well as the phenomenological bond charge model developed by Weber to describe a peculiar dispersion of the TA phonon in tetrahedral semiconductors.[15]

According to Weinstein *et al.* the photoelastic parameter χ' defined by[16]

$$\chi' = -\frac{\partial \ln(\epsilon - 1)}{\partial \ln \Omega} \tag{1}$$

serves as an indicator of the dimensionality of the bonding network of a solid, where ϵ is the infrared dielectric constant and Ω the volume per molecule; the network dimensionality means the number of dimensions in which the covalently bonded molecular unit is macroscopically extended. In amorphous and molecular chalcogenide materials, the compression mainly increases the broadening of electronic bands through the enhancement of the coupling between molecules. This effect leads to the change in the dielectric response to give $\chi' > 1$. On the other hand, the change in the dielectric response of a semiconductor with the three-dimensional network of tetrahedral bonding (hereafter abbreviated as 3D semiconductor) is determined by the increase in the bonding-antibonding energy gap to give $\chi' < 0$.

A layered semiconductor consists of two types of chemical bonding, depending on the crystallographic orientation. The layer itself can be regarded as a molecule, whereas the bonding within the layer is covalent or partially ionic. In this sense, a layered material is expected to

be two-dimensional. We find it of interest to see how such a dual character in the electronic state of a layered material varies with contraction of its volume. Weinstein *et al.*[17] have deduced $\chi'=1.6$ for layered GeS_2. Polian *et al.* have measured the Raman scattering and photoelastic properties of GaS under hydrostatic pressure.[18,19] Their data show that $\chi'\simeq 1$ and a zone-boundary TA mode softens with a rate of -1.0×10^{-2} GPa^{-1}. No systematic study, however, has been made, and consequently no correlation of χ' with the network dimensionality has yet been established for layered materials.

In the present paper, we report Raman scattering studies of $2H(\varepsilon)$-GaSe under hydrostatic pressure up to 3.4 GPa. Contrary to the $2H(\beta)$ polytype of GaS, the $2H(\varepsilon)$ polytype of GaSe has no inversion symmetry, and thereby the TO and LO modes are Raman active in addition to other nonpolar optical modes. One may evaluate the Born effective charge from the LO-TO splitting. The pressure dependence of the Raman spectrum of nonpolar modes gives information on the variation of the interlayer force and the intralayer bond-bending force. We have also measured the pressure dependence of the infrared dielectric constant by observing the interference fringe spectrum. It manifests the pressure dependence of the photoelastic parameter and the average gap, which reflect the nature of the electronic structure. The present paper deals with properties of the chemical bonding of GaSe on the basis of these experimental results.

II. EXPERIMENTAL

The single crystal has been grown by the Bridgman method. The crystal is cleaved into the thickness of 0.01—0.1 mm, and cut into the typical area of 0.3×0.3 mm^2. It is immersed in the 4:1 mixture of methanol and ethanol in the pressure cell of a metal-gasketed diamond-anvil apparatus. The thickness of the gasket is 0.25 mm and the diameter of the hole is 0.4 mm. The pressure is calibrated by measuring the wavelength shift of the R_1 luminescence line of a chip of ruby crystal irradiated by a Kr laser or a He-Ne laser.

The Raman scattering spectrum is measured in the backscattering geometry from the basal plane of the crystal. The 647.1- and 676.4-nm lines of a Kr laser are employed as light sources. The laser beam is focused into a diameter of 0.1—0.2 mm on the sample surface. The spectrometer consists of a Nalumi 1000D-WN double monochromator equipped with holographic gratings, a Hamamatsu R943 photomultiplier, and a conventional photon-counting system.

The refractive index is measured for the electric field **E** of radiation normal to the **c** axis by observing the interference fringe spectrum in the wavelength range of 0.6—1.3 μm. The spectrum is observed by the lock-in method with a Nikon G250 monochromator, a halogen lamp, and a Hamamatsu P397 PbS detector. All measurements are performed at room temperature.

The $2H(\varepsilon)$-GaSe crystal belongs to the $D^1_{3h}(P\bar{6}m2)$ space group and has the following normal modes:[20]

$$\Gamma=4A'_1+4A'_2+4E'+4E'' , \quad (2)$$

where one A'_2 and one E' are acoustic modes. The A'_1, E', and E'' optical modes are Raman active. A'_1 modes have the symmetry property of $xx+yy$ and zz; E', of xy and xx-yy; and E'', of zx and yz. Because of these symmetry properties, nonpolar A'_1 and E' modes may be observed in the present experimental geometry as shown by the path A in Fig. 1. Figure 2 shows the pressure dependence of the spectrum measured by the use of the 676.4-nm line of a Kr laser. The spectrum which has been measured in the atmosphere with a wide and 0.2-mm-thick crystal is also shown for comparison in Fig. 2. Observed Raman lines are assigned with reference to the literature.[21]

Among them, the E'(LO) mode should be observed only in the forward scattering geometry because it propagates along the basal plane, and thereby has a vanishing momentum along the c axis. However, the radiation scattered by the E'(LO) mode may be reflected backwards at the sample surface as shown by the path B in Fig. 1. This reflection allows us to observe the E'(LO) mode in the backscattering geometry.

According to the symmetry properties mentioned above, E'' modes are active in zx and yz polarizations of incident and scattered radiations. In practice, two E'' modes are observable in these polarizations as can be seen in Fig. 2. The radiation scattered by an E'' mode is polarized parallel to the c axis and propagates within the basal plane in the present experimental geometry. Therefore, the Raman intensity is very weak if measured with a large crystal in the usual way. However, if the sample is mounted in the diamond-anvil cell, the scattered radiation may be emitted out of the cell through a reflection at the wall of the gasket as shown by path C in Fig. 1, so that the E'' lines become intense. These E'' lines are attenuated abruptly at a certain pressure depending on the wavelength of the laser beams. Figure 3 shows the pressure dependence of the intensity of the E'' mode at ~ 60 cm^{-1} relative to the E' mode at 20 cm^{-1}. The threshold is 0.4 GPa for the 647.1-nm laser beam and 1.1 GPa for the 676.4-nm beam.

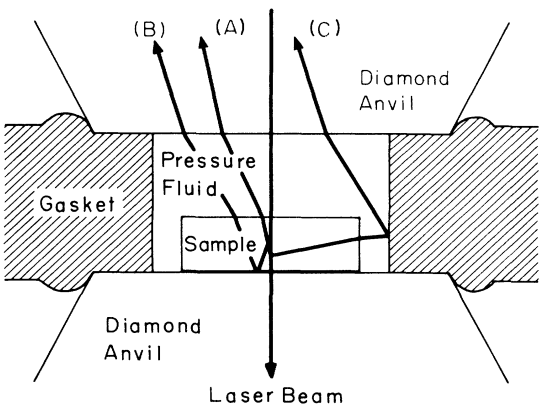

FIG. 1. Various paths of the Raman scattered radiation which is emitted backwards out of the diamond-anvil cell.

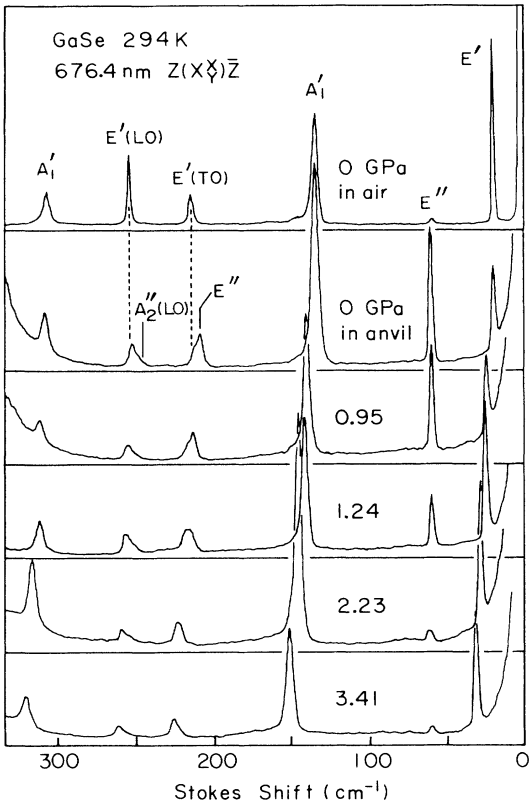

FIG. 2. Pressure dependence of the unpolarized Raman spectrum of GaSe measured in the backscattering geometry with the 676.4-nm beam of a Kr ion laser at 294 K.

At ambient conditions, the indirect edge of the fundamental optical absorption lies at some 1.95 eV,[22] which is barely higher than the photon energy, 1.916 eV, of the 647.1-nm radiation. This indirect gap is between the valence-band maximum at the Γ point and the conduction-band minimum at the M point.[23] According to Besson *et al.* the indirect absorption edge shifts towards lower energy with a rate of -0.11 eV GPa^{-1}.[22] Similar to the anisotropy of absorption at the direct edge,[24] the indirect absorption would be much stronger for $\mathbf{E}\|\mathbf{c}$ than for $\mathbf{E}\perp\mathbf{c}$. The radiation scattered by an E'' mode is polarized with $\mathbf{E}\|\mathbf{c}$. It is to be selectively absorbed if the pressure is high enough to let the indirect edge approach its photon energy. The radiation can hardly be emitted out of the sample if the absorption coefficient amounts to the order of 100 cm^{-1}. This effect causes an abrupt decrease in the intensity of the E'' mode at a certain pressure. The threshold pressure is higher by 0.7 GPa for the 676.4-nm beam than for the 647.1-nm beam. The pressure coefficient of the indirect edge as estimated from this observation is -0.12 eV GPa^{-1}, being in good agreement with the previous absorption experiment.[22]

Figure 4 shows the pressure dependence of the Stokes shifts of the Raman lines. Most lines shift towards higher frequency as the pressure increases. The initial frequency and the pressure coefficient of each line are tabulated in Table I. The results of a previous measurement under pressure up to 0.85 GPa are also tabulated for comparison.[25] One may note that the pressure coefficient of the E'(LO) mode is smaller than the E'(TO) mode: The magnitude of the LO-TO splitting decreases with a pressure coefficient of -6.0×10^{-2} GPa^{-1}. The E'' mode observed at 59 cm^{-1} at atmospheric pressure shifts initially to 60 cm^{-1}, but remains at almost the same frequency under high pressures.

Figures 5 and 6 show the pressure dependence of the interference fringe spectrum near and ~1 eV below the fundamental absorption edge, respectively. The interference fringes shift remarkably towards shorter wavelength with pressure. This behavior indicates that the product nc decreases with pressure, where n and c are refractive index and the lattice constant of the c axis, respectively. The experimental values of the fractional change, $\Delta(nc)/n_0c_0$, are plotted as a function of pressure in Fig. 7. The variation is rather nonlinear and independent of the wavelength of radiation.

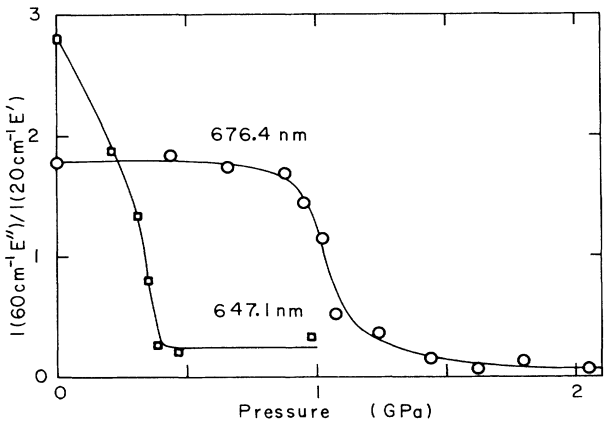

FIG. 3. Pressure dependences of the relative intensity of the E'' mode at ~60 cm^{-1} to the E' mode at ~20 cm^{-1} for 676.4- and 647.1-nm laser beams.

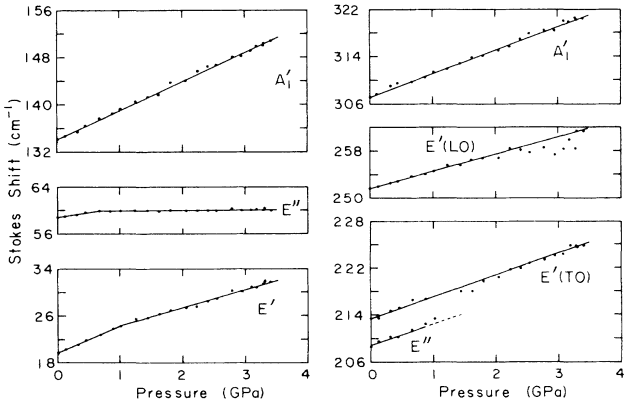

FIG. 4. Pressure dependence of the Stokes shift of the Raman lines in GaSe.

TABLE I. Wave number, $\bar{\nu}_{i0}$, of phonons in GaSe and GaAs at the atmospheric pressure and pressure coefficient of the Raman active phonons in GaSe.

Mode		$\bar{\nu}_{i0}$ (cm^{-1})		$d\bar{\nu}_i/\bar{\nu}_{i0}dP$ in GaSe (10^{-2} GPa^{-1})	
GaSe	GaAs	GaSe	GaAs	Present work	Ref. 25
A_1'	LO_Γ	307.1±1	292[a]	1.30	1.4
E'(LO)		251.5±1		1.19	1.2
A_2''(LO)		247[b]			
	$LO_{L/2}$		269[a]		
A_2''(TO)		236[b]			
E'(TO)	$TO_{L/2}$	213.3±1	265[a]	1.76	
E''	TO_Γ	208.7±1	269[a]	2.06	2.1
A_1'	$LA_{L/2}$	134.0±1	130[a]	3.73	4.3
				2.83 ($P<0.6$ GPa)	
E''		59.0±1		0.16 ($P>1$ GPa)	1.7
E''	$TA_{L/2}$	55.4±1	53[a]		
				23.4 ($P<1$ GPa)	
E'		19.7±1		12.6 ($P>1$ GPa)	23.2

[a]Reference 30.
[b]Reference 21.

III. DISCUSSION

A. Dispersion of phonons

Before we proceed to the discussion of the present experimental results, we briefly mention the nature of the GaSe crystal which is revealed in the phonon dispersion. This crystal has the structure as shown in Fig. 8. A layer consists of four sublayers: two Ga sublayers are sandwiched between a pair of Se sublayers. They are bound to each other by the threefold Se-Ga and the onefold Ga-Ga bondings. Each Se atom is coordinated by three Ga atoms and lone pair electrons directed towards outside of the layer.[26,27] A layer is bound to adjacent layers by weak electrostatic forces. In short, the intralayer chemical bondings may be regarded as quasitetrahedral. The sequence of sublayers may be represented as

$$\cdots X—M—M—X \cdots X—M—M—X \cdots ,$$

where X and M denote the anion and the cation sublayers, respectively; the dotted and solid lines denote interlayer and intralayer bondings, respectively.

Figure 9 schematically shows the dispersion along the [001] direction derived on the basis of the Raman data at the atmospheric pressure. Like the $\Gamma—A$ dispersion in a

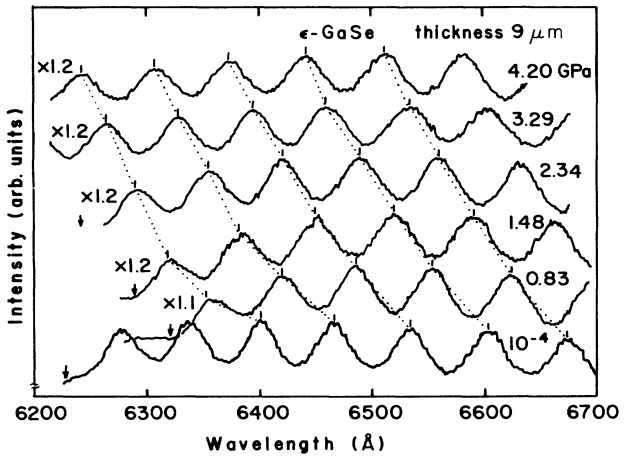

FIG. 5. Pressure dependence of the interference fringe spectrum near the fundamental absorption edge of a GaSe crystal with thickness of 9 μm.

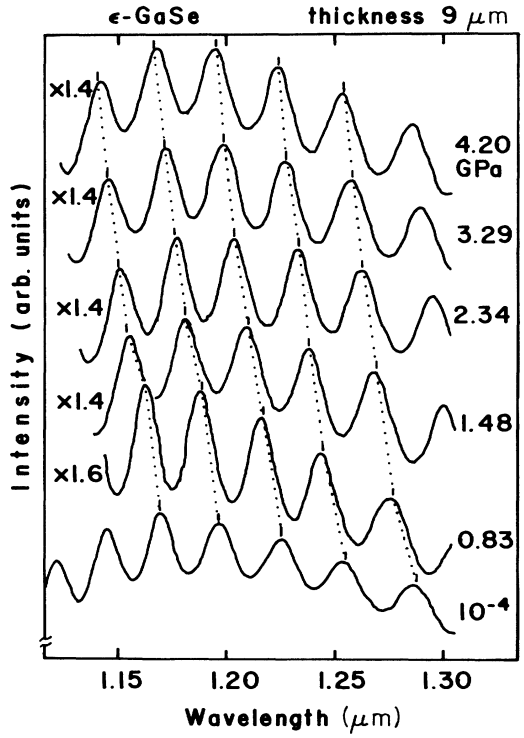

FIG. 6. Pressure dependence of the interference fringe spectrum in the near-infrared transparent region of GaSe for the same sample as in Fig. 5.

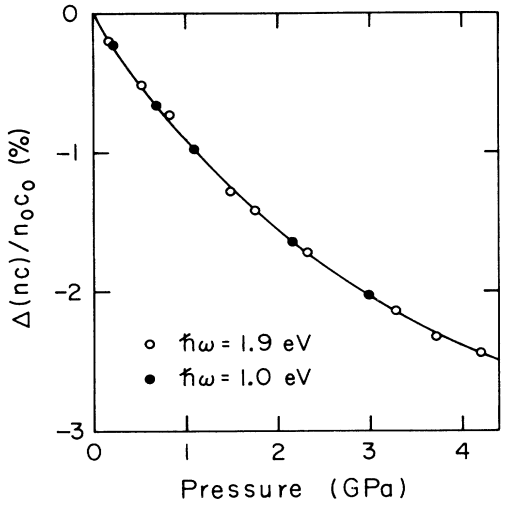

FIG. 7. Fractional variation of the product nc with pressure.

wurtzite-type compound, the phonon dispersion along the [001] direction in GaSe may be analogous with that along the [111] direction in the zinc-blende-type compounds. There is, however, a striking difference in the arrangement of the X-M pair from a 3D semiconductor in which X and M sublayers are arranged as

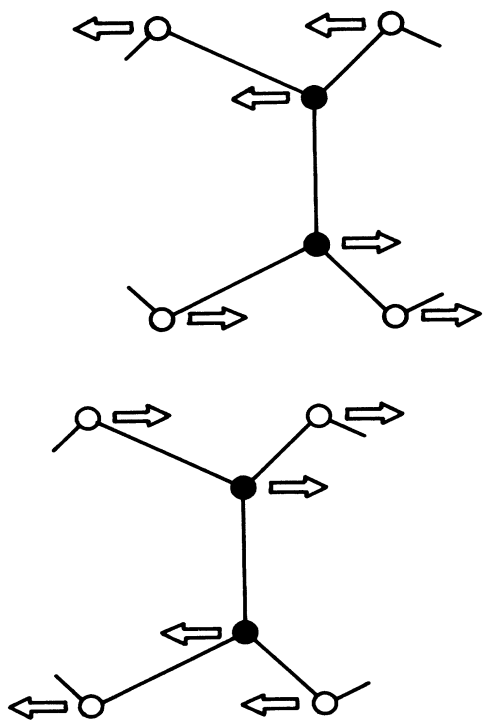

FIG. 8. Projection of the crystal structure of GaSe on the $(11\bar{2}0)$ plane. Open and solid circles represent Se and Ga atoms, respectively. Arrows are dislacement vectors of the $E''(ta_1)$ mode.

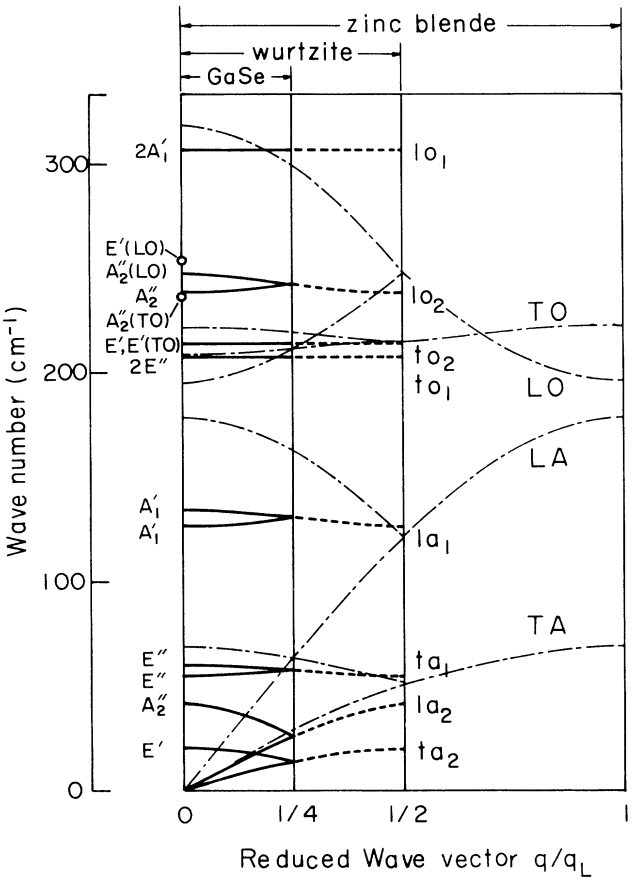

FIG. 9. Correspondence in energy and mode of the phonon dispersion in GaSe with that in a 3D semiconductor. Solid lines show the dispersion along the [001] direction in the $2H(\varepsilon)$ polytype of GaSe, Dashed lines are dispersion curves expected for a polytype with a one-layer periodicity of stacking sequence. Dashed-dotted lines show dispersions along [001] and [111] directions in hypothetical wurtzite- and zinc-blende-type structures, respectively.

$$-X-M-X-M-X-$$

along the [111] direction: The arrangement of the X-M pair is reversed by every two pairs in GaSe. This difference gives rise to a splitting of every phonon branch at the midpoint of the Γ-L line of the zone scheme of the zinc-blende structure. Adjacent M sublayers vibrate out of phase and X sublayers vibrate in phase in one of the split-off branches, whereas M sublayers vibrate in phase and X sublayers vibrate out of phase in the other branch. A similar splitting takes place in a semiconductor superlattice.[28] These split-off modes are denoted as ta_1,ta_2 and so on in Fig. 9. The subscripts 1 and 2 refer to the modes in which cations and anions vibrate out of phase, respectively. In the $2H(\varepsilon)$ polytype, these modes are folded to the Γ point because of the two-layer periodicity of the stacking of layers.

The splitting is very large in comparison with a semiconductor superlattice because the $X\cdots X$ bonding is

very weak. Besides, the dispersion of every branch along the [001] direction becomes very small. Because of the relative phase of atomic displacements,[29] ta_2, la_2, to_1, and lo_1 modes are expected to have frequencies comparable to those of TA, LA, TO, and LO modes, respectively, at the Γ point of a zinc-blende–type semiconductor, if the X—M and M—M bondings are covalent or partially ionic. Similarly, ta_1, la_1, to_2, and lo_2 should have frequencies comparable to those of corresponding modes at the midpoint of the Γ—L line of a zinc-blende–type material. Because of the proximity of atomic masses of anion and cation, GaAs is the most appropriate material to test the validity of these correspondence relationships. We refer to the neutron scattering data by Waugh and Dolling for the phonon dispersion in GaAs.[30] Table I shows a comparison of phonon frequencies between GaSe and GaAs. A good correspondence is found to exist between the two materials.

As for $E'(ta_2)$ and $A_2''(la_2)$ modes, entire layers vibrate almost rigidly.[29] Frequencies of these external modes are determined by either the shear or the compressional component of the interlayer restoring force, particularly due to the $X\cdots X$ bond. The $E'(ta_2)$ mode is Raman active. Its frequency serves as a probe for the character of the $X\cdots X$ bond. It is discussed quantitatively in the following subsection.

B. The pressure dependence of the interlayer bonding

The frequency, ω_1, of the $E'(ta_2)$ mode is given in the rigid layer approximation by

$$\omega_1=\left[\frac{W^s}{m_X+m_M}\right]^{1/2}, \tag{3}$$

where W^s is the force constant for the shear vibration, and m_X and m_M are atomic masses of anion and cation, respectively. Figure 10 shows the variation of W^s with pressure. The initial value of the pressure coefficient $\partial \ln W^s/\partial P$ is found to be 0.54 GPa^{-1}, which is an order of magnitude larger than the coefficients of intralayer force constants estimated from the variation of $E'(TO)$ and A_1' modes.

The electrostatic potential Φ_k associated with the kth Se$\cdots$Se bond may be expressed in terms of the Born repulsion and the van der Waals attraction as follows:

$$\Phi_k=Be^{-r_k/\rho}-Cr_k^{-6}, \tag{4}$$

where r_k is the Se$\cdots$Se bond length, ρ is the hardness parameter, and B and C are the coefficients of respective potential terms to be determined. The stretching force constant, F_k, of this bond is given by

$$F_k=\frac{B}{\rho^2}e^{-r_k/\rho}-42Cr_k^{-8}. \tag{5}$$

Φ_k is anharmonic so that F_k depends strongly on r_k. The Se$\cdots$Se bonding is threefold. If the interlayer interactions of a Se atom with second and more distant neighbors are neglected for simplicity, the force constant W^s relates to F_k as

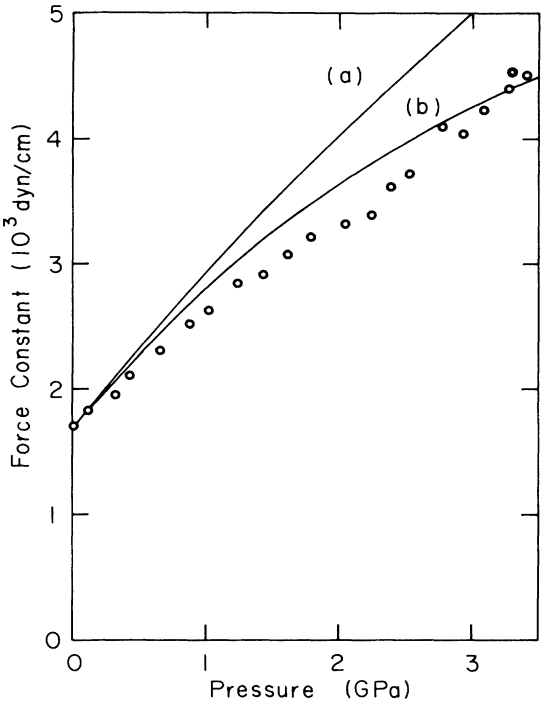

FIG. 10. Pressure dependence of the force constant associated with the interlayer Se$\cdots$Se bond. Circles are experimental values and solid lines are theoretical curves. (a) and (b) refer to the case a and the case b, respectively, with respect to the value of G_0', adopted in evaluating the c parameter from Eq. (8).

$$W^s=2F_k\sin^2\theta, \tag{6}$$

where θ is the angle between a Se$\cdots$Se bond and the c axis. The hardness parameter ρ is known to be 0.34 Å for monovalent halogen ions without regard to the species.[31]

We have $r_k=3.88$ Å at atmospheric pressure.[32] The radius 1.94 Å of the Se atom is close to Pauling's radius 1.96 Å of a Br^- ion. This fact allows us to adopt $\rho=0.34$ Å. We also have $\sin\theta=0.822$ and $W^s=1.70\times10^3$ dyn cm^{-1} at the atmospheric pressure. Then, with the aid of the equilibrium condition

$$\frac{\partial\Phi_k}{\partial r_k}=0, \tag{7}$$

we obtain $B=7.08\times10^{-9}$ erg and $C=5.08\times10^{-58}$ erg cm^6. The value of B agrees well with 9.04×10^{-9} erg which can be evaluated from the Huggins-Mayer parameters for a pair of Br^- ions.[31] The value of C is comparable to 2.0×10^{-58} erg cm^6 for Br^- ions in alkali halide crystals,[31] 2.13×10^{-58}erg cm^6 for Kr atoms, and 5.09×10^{-58} erg cm^6 for Xe atoms.[33] Katahama *et al.* have obtained $C=7\times10^{-58}$ erg cm^6 for iodines in $4H$-CdI_2 from an experimental study similar to the present one.[34]

Experimental data of the pressure dependence of lattice parameters are necessary to evaluate r_k and θ under pressure. However, only the low-pressure compressibilities $\kappa_{\parallel 0}=0.026$ GPa^{-1} for the c axis and $\kappa_{\perp 0}=0.005$ GPa^{-1}

for the a axis are available to date for GaSe.[35,36] The c axis of InSe is known to obey a modified Murnaghan equation of state

$$\frac{c}{c_0}=\left[1+\frac{G_0'P}{G_0}\right]^{-1/(3G_0')}, \tag{8}$$

with $G_0=1/(3\kappa_{\|0})$ and $G_0'=10.8$,[37] where P is the pressure and G_0' is the pressure derivative of G_0. Polian *et al.* have reported experimental values of c/c_0 and a/a_0 in GaS.[19] We find that their data of c/c_0 is well reproduced by Eq. (8) with $G_0'=7.5$. Their data also show that a/a_0 varies almost linearly as

$$\frac{a}{a_0}=1-\kappa_{\perp 0}P \tag{9}$$

under pressure up to 20 GPa. The x-ray diffraction study of GaS by d'Amour *et al.* has shown that, though a polytype transition takes place at some 2 GPa, the thickness of the layer has a compressibility of 0.005 GPa^{-1}.[38] This value is close to $\kappa_{\perp 0}$. With reference to this experimental information on InSe and GaS, we will employ the c parameter calculated from Eq. (8) with $G_0'=7.5$ (case a) and 10.8 (case b) in the following discussion, and assume that the compressibility of the a axis is independent of pressure in the present experimental range and the thickness of the layer has the same compressibility as the a axis.

The value of W^s calculated from Eq. (6) with these lattice parameters are compared with experimental values in Fig. 10. Both calculated curves rate somewhat larger than experimental results, but reproduce well the overall behavior of W^s. Our calculation neglects second neighbor and more distant interactions. Those terms might yield a smaller variation of W^s. It is worthwhile to mention that low-frequency external modes in molecular chalcogenide solids also have large pressure coefficients. For instance, the initial value of $\partial \ln\omega/\partial P$ is reported to be 0.20 GPa^{-1} in As_4S_4,[39] and 0.28 GPa^{-1} in P_4S_3,[40] which are in good accordance with 0.234 GPa^{-1} for the $E'(ta_2)$ mode in GaSe.

C. Intralayer bond-bending force

The ta_1 mode has the E'' symmetry. Displacement vectors of this mode are shown in Fig. 8. The sublayers which are identical under translation of a layer to the adjacent one vibrate out of phase against each other. A strong cancellation of the differential polarizability takes place in such a mode, so that the Raman cross section is very small.[41] The Davydov conjugate partner corresponds to the TA mode at the L point of the zone scheme of the zinc-blende structure as noticed from Fig. 9. This mode also has the E'' symmetry in GaSe. It has a finite cross section because all sublayers identical under transformation of layers vibrate with the same phase, and is observed at 59 cm^{-1} at the atmospheric pressure. The frequency is dominated by the interlayer force associated with a Se $\cdots$ Se bond as well as the intralayer bond-bending force. Nevertheless, the experimental frequency varies very little. This implies that the intralayer bond-bending force weakens so as to compensate a large increase in the strength of the interlayer force.

A coupled oscillator model holds well among these Davydov conjugate E'' modes and the E' mode.[29,42] Let the frequencies of the $E''(ta_1)$ mode and its Davydov partner be ω_2 and ω_3, respectively. Then we have a relation

$$\omega_2=(\omega_3^2-\omega_1^2)^{1/2}. \tag{10}$$

Figure 11 shows the pressure dependence of ω_2 calculated from Eq. (10) with experimental values of ω_3 and ω_1. The $E''(ta_1)$ mode softens linearly with a pressure coefficient of -2.9×10^{-2} GPa^{-1}. The Se $\cdots$ Se bonding retains the van der Waals–type character even under high pressures, as argued in Sec. III B. In this situation, valence electrons may hardly transfer between adjacent layers even if the Ga—Ga bond is bent. The van der Waals interaction merely serves as the pressure transmitting medium upon an isolated layer as far as the $E''(ta_1)$ mode is concerned. That is, the bond-bending force which determines the frequency of the $E''(ta_1)$ mode is strictly short range along the c axis. The compressibility of a layer, $\kappa_l\simeq 3\kappa_{\perp 0}=0.015$ GPa^{-1}, yields the Grüneisen parameter $\gamma=\kappa_l^{-1}\partial \ln\omega_2/\partial P$ of -1.9. The bond-bending force crucial to the behavior of a short-wavelength TA mode in a zinc-blende-type semiconductor is known to be short range as well. Correspondingly, one may expect that it has a similar Grüneisen parameter. Indeed, we have $\gamma=-1.7$ and -1.5 for the TA_L mode in GaAs and ZnSe, respectively.[43]

D. The Born effective charge and photoelastic parameter

In order to deduce the Born effective charge and the photoelastic parameter, we evaluate ϵ from our experimental data of $\Delta(nc)/n_0c_0$ shown in Fig. 7. The results are shown in Fig. 12 along with calculated curves of $\Delta c/c_0$ and $\Delta\Omega/\Omega_0$. The fractional decrease in nc is smaller by a factor of about 2 than that in c. This is because the dielectric constant $\epsilon=n^2$ *increases* with pressure in quite a contrast to the case of a 3D semiconductor.

The Born effective charge e_T^* which is given by

$$e_T^*=[\mu\Omega\epsilon(\omega_{\rm LO}^2-\omega_{\rm TO}^2)/(4\pi e^2)]^{1/2} \tag{11}$$

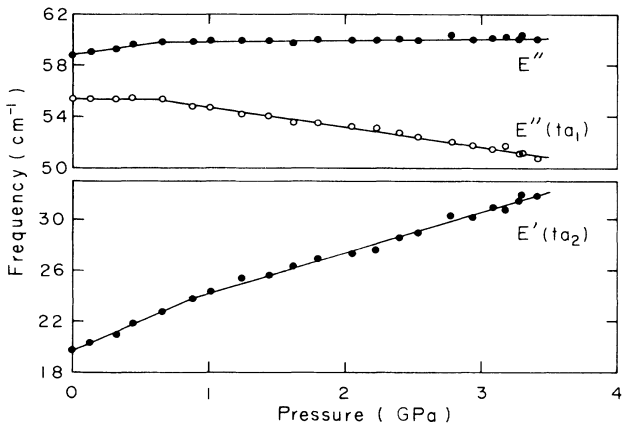

FIG. 11. Pressure dependence of the lowest-lying three modes. Solid and open circles are experimental and calculated values, respectively.

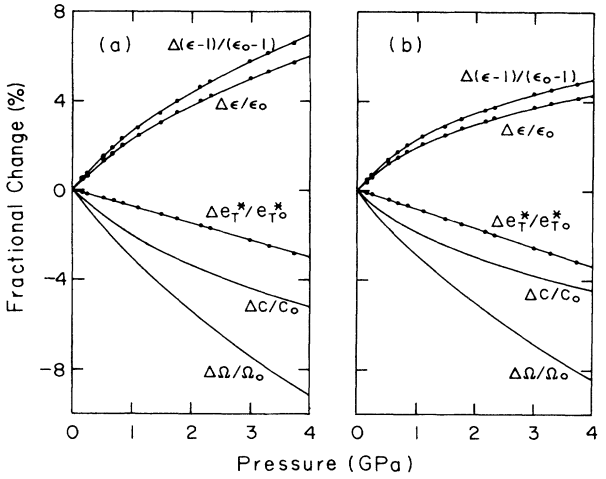

FIG. 12. Pressure dependence of the crystal colume (Ω), the c parameter, the Born effective charge (e_T^*), the infrared dielectric constant (ϵ), and $\epsilon-1$. Solid circles are experimental values. As for (a) and (b), see the caption of Fig. 10.

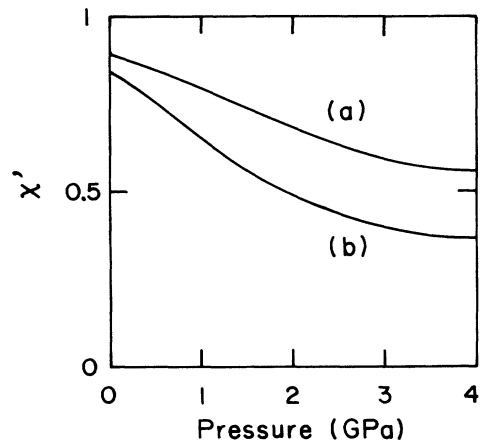

FIG. 13. Pressure dependence of the photoelastic parameter. As for (a) and (b), see the caption of Fig. 10.

is a measure of the change in the charge distribution. μ, $\omega_{\rm LO}$, and $\omega_{\rm TO}$ in Eq. (11) refer to the reduced mass of a cation-anion pair, the frequency of the LO mode, and the frequency of the TO mode, respectively. From our Raman scattering experiments, we have

$$\partial \ln(\omega_{\rm LO}^2-\omega_{\rm TO}^2)/\partial P=-5.7\times10^{-3}\ {\rm GPa}^{-1}$$

for the polar E' mode. This value yields Δe_T^* as in Fig. 12. e_T^*, and thus the ionicity, decreases rather linearly with pressure. The slope yields $\kappa_l^{-1}\partial \ln e_T^*/\partial P=-0.5$ (case a) to -0.6 (case b), which agrees well with the Grüneisen parameter of e_T^* in 3D semiconductors, e.g., -0.5 in GaAs and -0.8 in ZnSe.[43] The linear dependence of e_T^* on pressure assures that a rearrangement of charge distribution takes place within individual layers.

We employ a smoothed curve of $\Delta(\epsilon-1)/(\epsilon_0-1)$ to obtain its pressure derivative needed to evaluate χ'. Figure 13 shows χ' thus obtained. χ' is close to unity at low pressures and decreases remarkably with pressure as if the molecular character of the interlayer bonding is continuously transformed into a covalent one. χ' remains, however, positive even above 4 GPa. In order to understand such a curious behavior of χ', we go back to the Penn-Phillips model from which Weinstein's criterion for the dimensionality of bonding network has evolved. The basic concept of this model may be expressed by the relation

$$\epsilon=1+\frac{AE_p^2}{E_g^2}\ , \tag{12}$$

where E_g, E_p, and A are the average bonding-antibonding energy gap, the plasma energy of valence electrons, and a numerical constant, respectively.[44] E_p^2 varies as Ω^{-1} with pressure. Thus the nonlinear behavior of χ' comes from the dependence of E_g on pressure. Figure 14 shows the variation of E_g deduced from the experimental data of ϵ.

Note that E_g increases superlinearly.

It is known that the dependence of an interband energy gap on hydrostatic pressure in GaSe and InSe may be described well in terms of anisotropic deformation potentials.[37] Let us denote the thickness of the layer as t and the van der Waals gap as w. Then if we apply this approach to E_g, its variation under hydrostatic pressure,

$$\Delta E_g=2\left[\frac{a_0\partial E_g}{\partial a}\right]\left[\frac{\Delta a}{a_0}\right]+\left[\frac{t_0\partial E_g}{\partial t}\right]\left[\frac{\Delta t}{t_0}\right]+\left[\frac{w_0\partial E_g}{\partial w}\right]\left[\frac{\Delta w}{w_0}\right] \tag{13a}$$

$$=2d_a\left[\frac{\Delta a}{a_0}\right]+d_t\left[\frac{\Delta t}{t_0}\right]+d_w\left[\frac{\Delta w}{w_0}\right], \tag{13b}$$

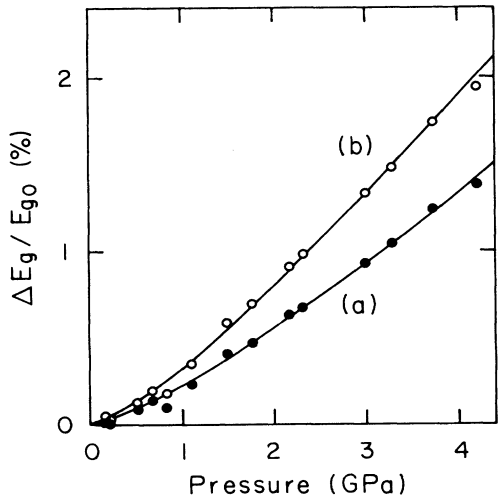

FIG. 14. Pressure dependence of the average energy gap of the Penn-Phillips oscillator. Solid and open circles are values deduced from experimental values of $\epsilon-1$ shown in Fig. 12. Solid lines are theoretical curves obtained from Eq. (14). As for (a) and (b), see the caption of Fig. 10.

may be expressed, taking $c=2(t+w)$ into account, as

$$\Delta E_g = D_a \left[\frac{\Delta a}{a_0} \right] + D_c \left[\frac{\Delta c}{c_0} \right] , \tag{14}$$

with

$$D_a = 2d_a + d_t - \frac{t_0}{w_0} d_w \tag{15a}$$

$$= 3d_l - \frac{t_0}{w_0} d_w \tag{15b}$$

and

$$D_c = \left[1 + \frac{t_0}{w_0} \right] d_w . \tag{16}$$

D_c does not represent the deformation potential for the change in the c axis. It is given by

$$d_c = \frac{(t+w)\partial E_g}{\partial(t+w)} = \frac{\kappa_\perp}{\kappa_{||}} d_t + \left[1 + \left[1 - \frac{\kappa_\perp}{\kappa_{||}} \right] \frac{t}{w} \right] d_w . \tag{17}$$

The first term of the right-hand side of Eq. (14) gives rise to a linear variation of E_g, while the second term gives rise to a nonlinear variation. We have $E_{g0}=6.33$ eV in GaSe.[26] Then the variation of $\Delta E_g/E_{g0}$ may be reproduced well by Eq. (14) with $D_a=-6.6$ eV and $D_c=0.90$ eV (case a), and $D_a=-8.7$ eV and $D_c=1.23$ eV (case b), as shown in Fig. 14. Substituting $t_0/w_0=1.50$ into Eqs. (15b) and (16),[32] we obtain $d_{l\perp}=-2.0$ eV and $d_{w\perp}=0.36$ eV (case a), and $d_{l\perp}=-2.7$ eV and $d_{w\perp}=0.49$ eV (case b): The subscript $\perp$ refers to the $\mathbf{E}\perp\mathbf{c}$ polarization with which the dielectric constant is measured.

The sign of D_c is positive. This property is common to molecular crystals. Though D_c is much smaller in magnitude than D_a, the compressibility of the c axis is very large at low pressures. The negative value of $D_c(\Delta c/c_0)$ almost cancels out the increase in E_g due to the compression of the volume of the layer, and renders $\chi' \simeq 1$ at low pressures. The compressibility of the c axis decreases rapidly with pressure. Consequently, χ' deviates significantly from unity under high pressures. Roughly speaking, $\chi'-1$ approaches asymptotically to $\sim 2D_a/3E_{g0}$ in the present case.

The static dielectric constant is determined by the imaginary part of the dielectric function via the Kramers-Kronig relation. A variety of interband transitions contributes to the dielectric function in GaSe, resulting in a broad band between 5 and 7 eV with subsidiary structures on the low-energy side and a sharp peak at 7.7 eV for $\mathbf{E}\perp\mathbf{c}$.[45] In brief, the bonding-antibonding energy gap of the Penn-Phillips model corresponds to the average over those resonance energies weighted by the oscillator strength.[46]

According to Weinstein *et al.*, the average energy gap in molecular chalcogenide solids originates mainly from transitions between nonbonding p states and antibonding states.[16] They have argued that the bulk deformation potential of this energy gap is 2.7 eV regardless of material. We find it of interest that $d_c < D_c \simeq 1$ eV in GaSe, even under low pressures where the interlayer contribution to d_c predominates over the intralayer contribution as can be seen from Eq. (17). Weinstein *et al.* ignore the volume factor which corresponds to t/w in a layered material. For the ring and the chain structures of S, Se, and Te examined by them, the volume occupied by intramolecular covalent bonds might be much smaller than the intermolecular space. In that case, $d_{w\perp}$ is more appropriate to be compared with their result. Besides, $d_{w\perp}$ is more definite in physical meaning than d_c. Anyhow, the interlayer and thus intermolecular deformation potential for GaSe is very small. This anomalous result is related to the electronic band structure of GaSe. The imaginary part of the dielectric function for $\mathbf{E}\perp\mathbf{c}$ owes primarily to optical transitions from $p_{x,y}$-like valence bands to s- and p_z-like conduction bands.[45] The $p_{x,y}$-like valence bands consist of well-defined bonding orbitals between Se and Ga within layer. Their energies are insensitive to the change in the van der Waals gap, causing $d_{w\perp}$ to be essentially small. The s- and p_z-like conduction bands may hybridize to a considerable extent with other p_z and s states, respectively, because of the uniaxial symmetry of the crystal structure. The hybridization makes the s-like conduction band susceptible to the change in the van der Waals gap. Furthermore it enhances the oscillator strength of the transition from $p_{x,y}$-like valence bands to the p_z-like conduction band. The finite value of $d_{w\perp}$ comes mainly from these hybridizations.

The energy gap between the $p_{x,y}$-like valence band and the lowest conduction band is minimum at the Γ point and gives rise to the optical absorption edge (A edge) for $\mathbf{E}\perp\mathbf{c}$. The highest valence band consists mainly of the Se p_z state and is raised 1–2 eV above the $p_{x,y}$-like valence band by the crystalline field anisotropy. This band also has the minimum direct gap (B edge) at the Γ point against the lowest conduction band. The dipole transition at the B edge is allowed for both $\mathbf{E}\perp\mathbf{c}$ and $\mathbf{E}||\mathbf{c}$ polarizations. However, the oscillator strength for $\mathbf{E}\perp\mathbf{c}$ is 2 orders of magnitude smaller than $\mathbf{E}||\mathbf{c}$ because the nonvanishing component of the matrix element for $\mathbf{E}\perp\mathbf{c}$ comes from an admixture of the $p_{x,y}$ states with the p_z-like valence band through the spin-orbit interaction.[47]

Authors have deduced deformation potentials for these direct edges in GaSe and InSe.[37] The results are tabulated in Table II along with the present results. One may note that $d_{w\perp}$ is very close to d_w^{cA}. This fact suggests that the energy of the lowest conduction band is rather insensitive to the change in the van der Waals gap with no regard of the position in the Brillouin zone.

On the other hand, the highest valence band is expected to have a nonbonding character like that in a molecular crystal because the Se p_z state takes dominant part in the lone pair orbit. This is justified by d_w^{cB} of 2.3 eV in InSe and 3.1 eV in GaSe, which agree well with 2.7 eV in molecular chalcogenide solids. One may expect that $d_{w||}$ of the average energy gap is as large as 2.7 eV because the transition from the Se p_z-like valence band to the conduction band is responsible for the infrared dielectric constant in the $\mathbf{E}||\mathbf{c}$ polarization.

According to Weinstein *et al.*, E_g in 3D semiconductors has deformation potential of values $\simeq -3.8$ eV for an average over a number of materials.[16] Values of $d_{l\perp}$ in

TABLE II. Interlayer and intralayer deformation potential (in eV) for fundamental energy gaps and the average energy gap in GaSe and InSe. Superscripts cB and cA refer to fundamental energy gaps at the B and A edges, respectively.

	GaSe	InSe
d_w^{cB}	3.1	2.30
d_w^{cA}		0.52
$d_{w\perp}$	0.43±0.07	
d_l^{cB}	−4.9	−9.3
d_l^{cA}		−4.4
$d_{l\perp}$	−2.4±0.4	

GaSe and d_l^{cA} in InSe are comparable to this value. It is confirmed from this result that the intralayer bonding in GaSe is quite similar to the tetrahedral bonding in 3D semiconductors.

IV. SUMMARY AND CONCLUSION

The Raman scattering and the infrared dielectric constant have been measured in the layered semiconductor GaSe under hydrostatic pressure up to 4 GPa. The results enable us to carry out a systematic study of the effect of pressure on the chemical bonding.

The pressure dependence of the frequency of an external mode has been interpreted in terms of the volume anharmonicity. The electrostatic potential involving the Born repulsion and the van der Waals attraction associated with the interlayer Se · · · Se bonding explains quantitatively the experimental results. It turns out that the character of the van der Waals bonding is retained even under high pressures.

An internal bond-bending mode corresponds in the displacement vectors to the TA mode at the midpoint of the Γ-L dispersion of a zinc-blende-type semiconductor. This mode softens remarkably with pressure. The LO-TO splitting of the polar E' mode and the infrared dielectric constant give the Born effective charge. Though the dielectric constant varies quite nonlinearly, the Born effective charge decreases almost linearly. These results indicate that the quasitetrahedral bonding within the layer tends to be destabilized by the delocalization and deformation of bond charges. It has been confirmed from the variation of the Raman intensity of the TA_L-like E'' mode that the lowest indirect energy gap decreases rapidly with pressure. This phenomenon could be closely related to the delocalization of the bond charge. The above results lead us to conclude that the chemical bonding in GaSe is similar to that in a tetrahedral semiconductor, while keeping an inherent molecular character of individual layers even under high pressures.

The dielectric constant yields the average energy gap between the bonding and the antibonding states. Our result shows that the energy gap increases superlinearly with pressure. The deformation potential approach allows us to describe this behavior in terms of individual contributions from the van der Waals and the intralayer bondings. It appears that the van der Waals bonding has a positive deformation potential reflecting the molecular character of the layer, whereas the intralayer bonding has a negative deformation potential characteristic of a partially ionic covalent bond. The coexistence of such molecular and covalent bondings causes the photoelastic parameter to be strongly dependent on pressure. One must take this effect into account in investigating the network dimensionality of an anisotropic solids. The present study demonstrates that the deformation potential for the bonding-antibonding energy gap, instead of the photoelastic parameter, leaves no ambiguity in the network dimensionality and, hence, gives a well-defined measure for characterizing the electronic structure.

ACKNOWLEDGMENTS

The authors wish to thank Mr. M. Sakai for his technical assistance during the course of experiments. This work was supported in part by a Grant-in-Aid for Scientific Research from the Ministry of Education, Science and Culture, Japan.

*Present address: Electronic Imaging and Devices Research Laboratory, Fuji Xerox Company, Ltd., Ebina 243-04, Japan.

[1]S. S. Mitra, O. Brafman, W. B. Daniels, and R. K. Crawford, Phys. Rev. **186**, 942 (1969).

[2]O. Brafman and S. S. Mitra, in *Light Scattering in Solids*, edited by M. Balkanski (Flammarion, Paris, 1971), p. 284.

[3]H. D. Hochheimer, M. L. Shand, J. E. Potts, R. C. Hanson, and C. T. Walker, Phys. Rev. B **14**, 4630 (1976).

[4]R. Trommer, E. Anastassakis, and M. Cardona, in *Light Scattering in Solids*, edited by M. Balkanski, R. C. C. Leite, and S. P. S. Porto (Wiley, New York, 1976), p. 396.

[5]R. Trommer, H. Müller, M. Cardona, and P. Vogl, Phys. Rev. B **21**, 4869 (1980).

[6]E. Aoki, E. Anastassakis, and M. Cardona, Phys. Rev. B **30**, 681 (1984).

[7]B. A. Weinstein, J. B. Renucci, and M. Cardona, Solid State Commun. **12**, 473 (1973).

[8]B. A. Weinstein and G. J. Piermarini, Phys. Rev. B **12**, 1172 (1975).

[9]B. A. Weinstein, Solid State Commun. **24**, 595 (1977).

[10]D. Olego and M. Cardona, Phys. Rev. B **25**, 1151 (1982).

[11]I. Ishida, J. Phys. Soc. Jpn. **39**, 1282 (1975).

[12]R. D. Turner and J. C. Inkson, J. Phys. C **11**, 3961 (1978).

[13]H. Wendel and R. M. Martin, Phys. Rev. Lett. **40**, 950 (1978); see also Phys. Rev. B **19**, 5251 (1979).

[14]G. Martinez, in *Handbook on Semiconductors*, edited by M. Balkanski (North-Holland, Amsterdam, 1980), Vol. 2, p. 181.

[15]W. Weber, Phys. Rev. Lett. **33**, 371 (1974).

[16]B. A. Weinstein, R. Zallen, M. L. Slade, and A. deLozanne, Phys. Rev. B **24**, 4652 (1981).

[17]B. A. Weinstein, R. Zallen, M. L. Slade, and J. C. Mikkelsen, Jr., Phys. Rev. B **25**, 781 (1982).
[18]A. Polian, J. C. Chervin, and J. M. Besson, Phys. Rev. B **22**, 3049 (1980).
[19]A. Polian and J. M. Besson, Phys. Rev. B **25**, 2767 (1982).
[20]N. Kuroda, Y. Nishina, and T. Fukuroi, J. Phys. Soc. Jpn. **28**, 981 (1970).
[21]J. C. Irwin, R. M. Hoff, B. P. Clayman, and R. A. Bromley, Solid State Commun. **13**, 1531 (1973); R. M. Hoff and J. C. Irwin, Phys. Rev. B **10**, 3464 (1974).
[22]J. M. Besson, R. Le Toullec, J. P. Pinceaux, A. Chevy, and H. Fair, High Temp. High Pressures **7**, 710 (1975).
[23]M. Schlüter, J. Camassel, S. Kohn, J. P. Voitchovsky, Y. R. Shen, and M. L. Cohen, Phys. Rev. B **13**, 3534 (1976).
[24]R. Le Toullec, N. Piccioli, M. Mejatty, and M. Balkanski, Nuovo Cimento **38B**, 159 (1977).
[25]E. A. Vinogradov, G. N. Zhizhin, N. N. Mel'nik, S. I. Subbotin, V. V. Panfilov, K. R. Allakhverdiev, S. S. Babaev, and V. F. Zhitar', Fiz. Tverd. Tela (Leningrad) **22**, 742 (1980). [Sov. Phys. Solid State **22**, 434 (1980)].
[26]N. Kuroda and Y. Nishina, J. Phys. Soc. Jpn. **50**, 2969 (1981).
[27]A. Nakanishi and T. Matsubara, J. Phys. Soc. Jpn. **51**, 3219 (1982).
[28]C. Colvard, R. Merlin, M. V. Klein, and A. C. Gossard, Phys. Rev. Lett. **45**, 298 (1980).
[29]T. J. Wieting and J. L. Verble, Phys. Rev. B **5**, 1473 (1972).
[30]J. L. T. Waugh and G. Dolling, Phys. Rev. **132**, 2410 (1963).
[31]M. P. Tosi, in *Solid State Physics,* edited by F. Seitz and D. Turnbull (Academic, New York, 1965), Vol. 16, p. 1.
[32]A. Kuhn, A. Chevy, and R. Chevalier, Phys. Status Solidi A **31**, 469 (1975).
[33]C. Kittel, in *Introduction to Solid State Physics,* 5th ed. (Wiley, New York, 1976), p. 77.
[34]H. Katahama, S. Nakashima, A. Mitsuishi, M. Ishigame, and H. Arashi, J. Phys. Chem. Solids **44**, 1081 (1983).
[35]M. Gatulle, M. Fischer, and A. Chevy, Phys. Status Solidi B **119**, 327 (1983).
[36]Y. Homma, M. Yamada, K. Yamamoto, and K. Abe, J. Phys. Soc. Jpn. **52**, 2777 (1983).
[37]N. Kuroda, O. Ueno, and Y. Nishina, J. Phys. Soc. Jpn. **55**, 581 (1986).
[38]H. d'Amour, W. B. Holzapfel, A. Polian, and A. Chevy, Solid State Commun. **44**, 853 (1982).
[39]R. Zallen and M. L. Slade, Phys. Rev. B **18**, 5775 (1978).
[40]T. Chattopadhyay, C. Carlone, A. Jayaraman, and H. G. von Schnering, Phys. Rev. B **23**, 2471 (1981).
[41]S. Nakashima, H. Katahama, Y. Nakahara, and A. Mitsuishi, Phys Rev. B **31**, 6531 (1985).
[42]Y. Yoshida, S. Nakashima, and A. Mitsuishi, Phys. Status Solidi B **59**, 655 (1973).
[43]B. A. Weinstein and R. Zallen, in *Light Scattering in Solids IV,* edited by M. Cardona and G. Güntherodt (Springer-Verlag, Berlin, 1984), p. 463.
[44]J. C. Phillips, in *Bonds and Bands in Semiconductors* (Academic, New York, 1973), p. 35.
[45]M. Piacentini, C. G. Olson, A. Balzarotti, R. Girlanda, V. Grasso, and E. Doni, Nuovo Cimento **54B**, 248 (1979).
[46]R. N. Nucho, J. G. Ramos, and P. A. Wolff, Phys. Rev. B **17**, 1843 (1978).
[47]N. Kuroda, I. Munakata, and Y. Nishina, Solid State Commun. **33**, 687 (1980).